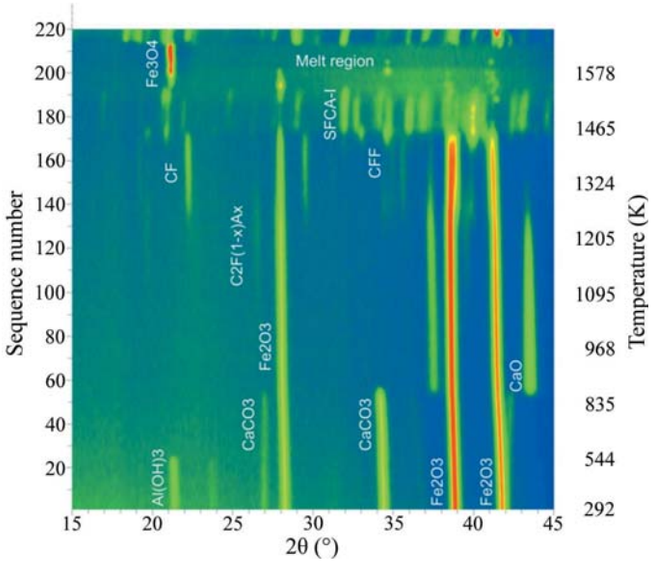

Figure 3.9.14
Raw *in situ* XRD data (Co $K\alpha$ radiation) collected during the synthesis of the iron-ore sinter bonding phase SFCA-I (Webster *et al.*, 2013). The data, collected as a function of heating temperature, are viewed down the intensity axis with red representing the highest intensity and blue the lowest intensity. The identified phases include gibbsite $Al(OH)_3$, calcite $CaCO_3$, haematite Fe_2O_3, lime CaO, calcium ferrites CF and CFF, calcium alumina-ferrite $C_2F_{1-x}A_x$, magnetite Fe_3O_4, and SFCA-I.

sinter bonding phase, SFCA-I, where SFCA = silico-ferrite of calcium and aluminium (Scarlett, Madsen *et al.*, 2004; Scarlett, Pownceby *et al.*, 2004; Webster *et al.*, 2013). The starting material, comprising a synthetic mixture of gibbsite, $Al(OH)_3$, haematite, Fe_2O_3, and calcite, $CaCO_3$, was heated to about 1573 K using an Anton Paar heating stage. The laboratory-based XRD data, collected using an Inel CPS120 diffractometer, are shown in Fig. 3.9.14, while the QPA results are shown in Fig. 3.9.15. Both figures show that there are several phase changes, including the formation of transient intermediate phases before the final production of SFCA.

In Fig. 3.9.15(*a*) the QPA results are derived using the Hill/Howard algorithm (Hill & Howard, 1987) in equation (3.9.26): this is the 'default' value reported by most Rietveld analysis software and normalizes the sum of the analysed components to 100 wt%. The apparent increase in haematite concentration at about 533 and 868 K results from the decomposition of gibbsite and calcite, respectively. There are no possible mechanisms in this system that could lead to an increase in haematite concentration at these temperatures; the reported increases are an artefact derived from normalizing the sum of all analysed phases to 100 wt%. Fig. 3.9.15(*b*) shows the correct result derived using the external-standard approach (O'Connor & Raven, 1988) embodied in equation (3.9.21), which has placed the values on an absolute scale. Fig. 3.9.15 demonstrates the importance of putting the derived phase abundances on an absolute scale for a realistic derivation of reaction mechanism and kinetics.

3.9.8. QPA using neutron diffraction data

One of the early papers detailing the application of the Rietveld method to quantitative phase analysis used neutron diffraction (ND) data (Hill & Howard, 1987). The reasons stated within this work define many of the advantages of neutrons over X-rays for diffraction in general and QPA in particular. One of the most significant advantages for QPA derives from the fact that neutrons interact weakly with matter, hence there is very little microabsorption with ND even in samples comprising a mixture of high- and low-atomic-number materials.

The high penetration capability of neutrons also enables the use of larger sample environments in *in situ* studies, thus enabling studies to be undertaken at, for example, higher pressures than would be possible with many X-ray sources. In addition, larger sample volumes can be investigated, which in turn produces better particle statistics and makes the technique less sensitive to grain size. It also makes ND a bulk technique in comparison with XRD, which is effectively surface-specific with a penetration depth of the order of microns or tens of microns.

The different strengths of ND and XRD mean that they can be exploited in combination to provide complementary information. For example, XRD generally has higher angular resolution and is therefore better at resolving small lattice distortions and heavily overlapped phases. However, the observed intensities in ND do not decrease as strongly with decreasing d-spacing. This results in ND providing more accurate determination of atomic displacement parameters and therefore the Rietveld scale factors; this then improves the accuracy of QPA derived from these scale factors (Madsen *et al.*, 2011).

Hill *et al.* (1991) have investigated the phase composition of Mg-PSZ (partially stabilized zirconia) using both ND and XRD. The surfaces of these materials were subjected to various treatments, which meant that they were no longer representative of the bulk. From the more highly penetrating ND data they obtained bulk properties including crystal structure and size and strain parameters of the components along with QPA. From XRD they were able to examine the surface of the samples to investigate the effects of surface grinding and polishing.

The majority of Rietveld-based QPA still relies on the use of accurate crystal structure models; consequently, it is of increasing importance that powder diffraction methods used for structure solution be robust and reliable. Combining laboratory or synchrotron XRD and ND has been shown to be of considerable benefit in the solution of complex structures *via* powder diffraction (Morris *et al.*, 1992). This joint-refinement approach has been used to determine the crystal structure of a component phase of Portland cement (De La Torre *et al.*, 2002) for subsequent use in Rietveld-based QPA.

One of the disadvantages of neutron sources is that they are much less accessible than laboratory X-ray sources and of much lower flux than either laboratory or synchrotron X-rays sources. In addition, larger samples are generally required; this is not always practical in the investigation of many materials.

In many phase systems, the presence of severe microabsorption in XRD data serves to limit the accuracy that can be obtained. The collection of ND data, where microabsorption is virtually absent, from selected samples provides more accurate QPA; selected ND-based values can therefore act as a benchmark for the more routine XRD-based studies.

3.9.9. QPA using energy-dispersive diffraction data

Energy-dispersive diffraction (EDD) involves the use of high-energy white-beam radiation, often from a synchrotron source. This provides very high penetration and is, therefore, ideal as a probe to examine the internal features of relatively large objects (Barnes *et al.*, 2000; Cernik *et al.*, 2011; Hall *et al.*, 1998, 2000). In an experimental arrangement such as that in Fig. 3.9.16, diffraction data can be measured by energy-dispersive detec-

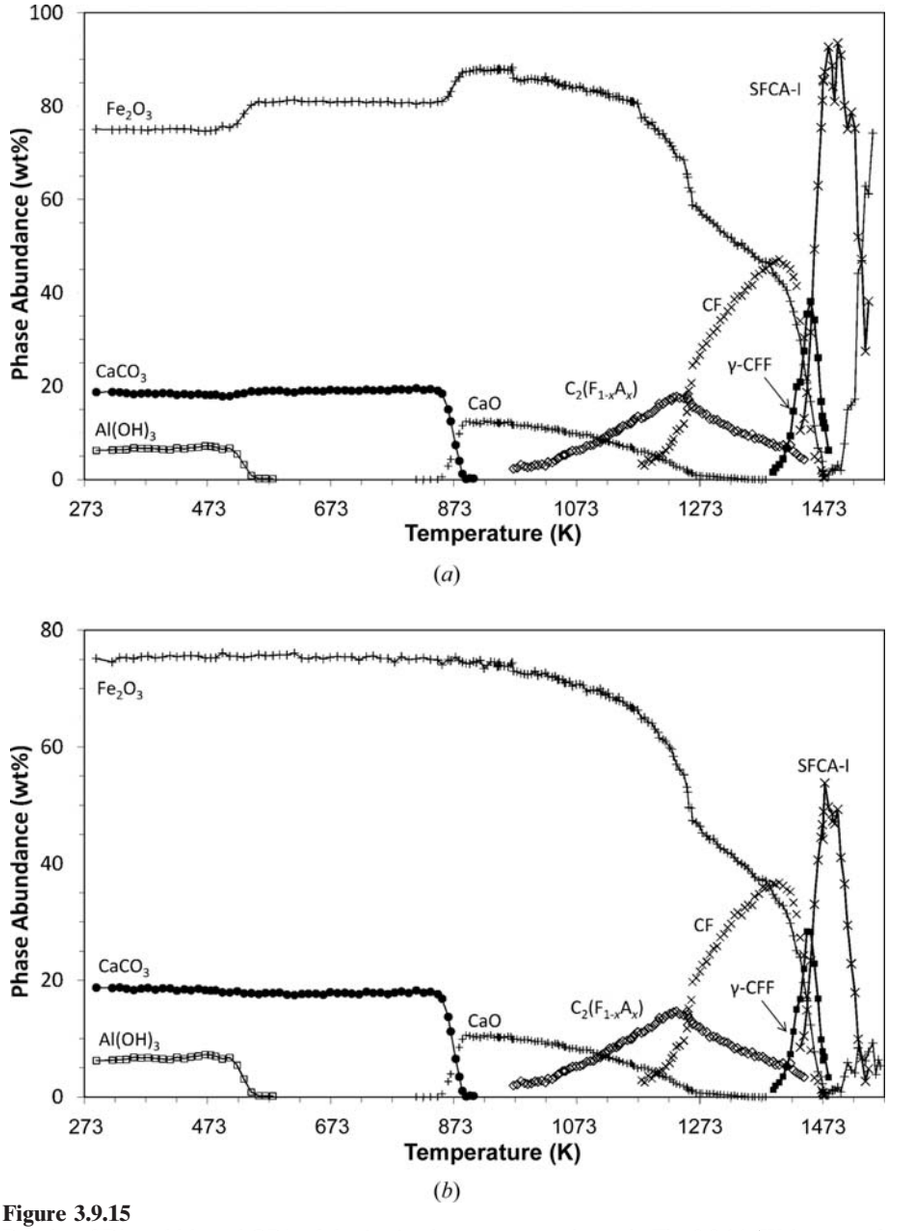

Figure 3.9.15
Results of Rietveld-based QPA of the *in situ* data sequence shown in Fig. 3.9.14 (Webster *et al.*, 2013). The relative phase abundances (upper) are derived using the Hill/Howard algorithm (Hill & Howard, 1987) in equation (3.9.26), while the absolute phase abundances (lower) have been derived from the external-standard approach (O'Connor & Raven, 1988) embodied in equation (3.9.21).

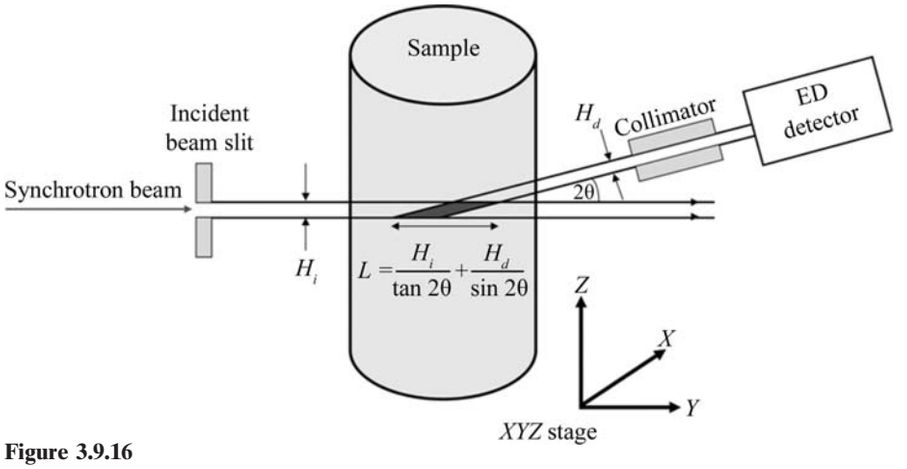

Figure 3.9.16
Basic experimental arrangement for energy-dispersive diffraction. The length of the active area or lozenge (dark grey region), L, is given by the function relating the incident- and diffracted-beam heights (H_i and H_d, respectively) and the angle of diffraction (2θ).

tors producing a spectrum of diffracted intensity as a function of energy.

Traditional angle-dispersive diffraction (ADD) satisfies Bragg's law by using a fixed wavelength and varying 2θ to map the d-spacings. In contrast, EDD data are collected directly on an energy scale at a constant 2θ and the energy is measured to map the d-spacings. This impinges upon the use of Rietveld methodology for QPA since, in contrast to ADD, the structure factors now vary as a function of energy. Energy is related to wavelength *via*

$$E\ (\text{keV}) = \frac{hc}{\lambda} \simeq \frac{12.395}{\lambda}, \qquad (3.9.46)$$

where E is the energy of the incident radiation in keV, h is Planck's constant, c is the speed of light and λ is the wavelength associated with that energy in ångstroms. Rearrangement of equation (3.9.46) and substitution for λ in Bragg's law enables the mapping of the measured energy scale to d-spacings:

$$E\ (\text{keV}) = \frac{6.197}{d \sin\theta}, \qquad (3.9.47)$$

where 2θ is the angle between the incident beam and the detector slit.

EDD data can be analysed using structureless profile-fitting methods such as those of Le Bail *et al.* (see Chapter 3.5) once the energy scale has been converted to a d-spacing scale (Frost & Fei, 1999; Larson & Von Dreele, 2004; Zhao *et al.*, 1997). If the distribution of intensities in the incident spectrum can be measured, it is possible to normalize the EDD data, correct for absorption and convert the pattern to an ADD form using a 'dummy' wavelength (Ballirano & Caminiti, 2001). Access to the incident spectrum, however, is not always possible, especially at synchrotron-radiation sources where the highly intense incident beam could damage the detector.

An alternative approach is to model the pattern directly on the energy scale *via* equation (3.9.47) (Rowles *et al.*, 2012; Scarlett *et al.*, 2009) and extract phase abundances using the methodologies described earlier in this chapter.

However, the major impediment to achieving this is the nonlinearity of the intensity distribution in the incident spectrum. This is due to (i) the nonlinear distribution of intensity as a function of energy in the incident beam, (ii) nonlinear detector responses (Bordas *et al.*, 1977) and (iii) absorption along the beam path (by the sample and air), which skews the energy distribution to the higher energies. This overall nonlinearity can be modelled empirically by functions such a lognormal

curve (Bordas *et al.*, 1977; Buras *et al.*, 1979) or by an expansion of a power function (Glazer *et al.*, 1978). Alternatively, it may be determined experimentally by the use of standards measured under the same conditions as the experiment (Scarlett *et al.*, 2009). This latter approach allows some separation of the contributions from the instrument and the sample, and allows some degrees of freedom in the refinement of sample-related parameters that may be of benefit in dynamic experiments. Other contributions to the diffraction pattern that must also be accounted for include any fluorescence peaks arising from the sample or shielding or collimators, and any detector escape peaks from both diffracted and fluorescence peaks. Fluorescence peak positions and relative intensities should be constant throughout the measurement and may therefore be modelled using a fixed 'peak group' whose overall intensity can be refined during analysis. Escape peaks can be accounted for by the inclusion of a second phase identical to the parent phase but with an independent scale factor and a constant energy offset determined by the nature of the detector (Rowles *et al.*, 2012).

Currently, few Rietveld software packages are capable of dealing directly with the differences between EDD and ADD, specifically (i) the variance of structure factors as a function of energy, (ii) the nonlinear distribution of intensity in the incident beam as a function of energy further modified by a nonlinear detector response, and (iii) the preferential absorption of lower-energy X-rays by the sample/air. *TOPAS* (Bruker AXS, 2013) embodies algorithms that allow the pattern to be modelled directly on the energy scale and also the inclusion of equations to account for intensity variations arising from the experimental conditions. This allows quantification from such data to be achieved directly using Rietveld-based crystal-structure modelling incorporating the Hill and Howard algorithm in equation (3.9.26) (Hill & Howard, 1987). The application of *TOPAS* to a complex EDD experiment investigating the changes to the anode during molten-salt electrochemistry conducted in molten $CaCl_2$ at about 1223 K has been described by Rowles *et al.* (2012) and Styles *et al.* (2012).

3.9.10. Improving accuracy

There are many factors that influence the accuracy and precision of QPA results where (i) accuracy is defined as the agreement between the analytical result and the true value, and (ii) precision is the agreement between results if the analysis is repeated under the same conditions. Precision may further be split into (i) repeatability, which is the agreement between repeated measurement and analysis of the same specimen, and (ii) reproducibility, which additionally includes re-preparation, measurement and analysis of the sample.

3.9.10.1. *Standard deviations and error estimates*

Determination of the actual accuracy of an analysis is not a trivial task in a standardless method. In fact, it cannot be achieved without recourse to another measure of the sample that does incorporate standards. Too often, analysts will report Rietveld errors calculated in the course of refinement as the errors in the final quantification. However, these numbers relate purely to the mathematical fit of the model and have no bearing on the accuracy of the quantification itself.

Consider, for example, a three-phase mixture of corundum, magnetite and zircon. Such a sample was presented as sample 4 in the IUCr CPD round robin on QPA (Scarlett *et al.*, 2002). Its components were chosen with the deliberate aim of creating a sample in which severe sample-related aberrations occur. Table 3.9.4 shows the weighed amounts of each component and the results of replicate analyses of three different sub-samples of this material.

Table 3.9.4
Comparison of errors generated during the analysis of XRD data (Cu $K\alpha$ radiation) from three sub-samples of sample 4 from the IUCr CPD round robin on QPA (Scarlett *et al.*, 2002)

The bias values are (measured − weighed) while the values denoted XRF are the phase abundances generated from elemental concentrations measured by X-ray fluorescence methods.

	Phase		
n = 3	Corundum	Magnetite	Zircon
Weighed	50.46	19.46	29.90
Mean XRD measured wt%	56.52	17.06	26.42
Mean of Rietveld errors	0.15	0.11	0.11
Standard deviation of measured wt%	0.63	0.41	0.35
Mean of bias	6.06	−2.58	−3.48
XRF	50.4(2)	19.6(1)	29.5(1)

It is apparent that the standard deviation of the mean abundances of the three replicates, which represents the expected precision in the analysis, is 3 to 4 times greater than the errors reported by the Rietveld software. The good level of fit achieved in conducting these analyses (evidenced by low R factors) could lead the analyst to conclude that the mean value ± the standard deviation of the mean is an adequate measure of the phase abundances and their errors.

However, both the Rietveld errors and the precision are at least an order of magnitude smaller than the bias. The large bias, in this case due to the presence of severe microabsorption, represents the true accuracy that can be achieved in this example. Unfortunately, there is nothing in the XRD data and Rietveld analysis process that indicates that there may be a problem. It is only when the QPA is compared with other estimates, in this case derived from XRF chemical-analysis results, that the problem becomes apparent. The analyst must take further steps to identify sample-preparation and/or data-collection protocols that may improve accuracy and, importantly, seek ways to verify the results.

3.9.10.2. *Minimizing systematic errors*

The fundamental measured quantities in a diffraction pattern are the integrated intensities of the observed peaks. The precision of these measurements can be improved by: (i) increasing the primary intensity of the diffractometer using optics or higher-power X-ray sources; (ii) using scanning linear detectors (see Chapter 2.1), which have multiple detector elements to collect individual intensities many times; these are then summed to achieve higher accumulated counts; (iii) increasing the number of counts accumulated at each step, that is increasing the step counting time T; and (iv) increasing the number of points, N, measured across the peak.

Often, the temptation is to collect data with large values of N and T to maximize counting statistics. However, the resulting increased precision is only useful up to the point where counting variance becomes negligible in relation to other sources of error; thereafter data-collection time is wasted. For example, if the sample is affected by the presence of severe sample-related